Journal of Power Sources 196 (2011) 8583–8589

Contents lists available at ScienceDirect

Journal of Power Sources

journal homepage: www.elsevier.com/locate/jpowsour

Surface-modified silicon nanowire anodes for lithium-ion batteries

Wanli Xu, Sri Sai S. Vegunta, John C. Flake*

Department of Chemical Engineering, Louisiana State University, Baton Rouge, LA 70803, USA

ARTICLE INFO

Article history:
Received 16 March 2011
Received in revised form 20 May 2011
Accepted 21 May 2011
Available online 27 May 2011

Keywords:
Solid electrolyte interphase
Lithium-ion battery
Anode
Silicon nanowire

ABSTRACT

Silicon nanowires with hydride, methyl and siloxane surfaces terminations were evaluated as anodes in lithium-ion half cells using $LiPF_6$ in EC/DMC electrolytes. Voltammetry, FT-IR and XPS analyses show hydride-terminated nanowires react with the electrolyte and methyl termination tends to passivate silicon surfaces. Silicon anodes pretreated with trimethoxymethylsilane show decreased lithium capacities similar to methylated anodes; however, the addition of 5% trimethoxymethylsilane as an electrolyte additive resulted in the formation of significantly more OPFx compounds while improving capacity retention relative to hydride-terminated nanowires (2348 mAh g^{-1} at 15 cycles at C/10 rates). FTIR analysis show trimethoxymethylsilane additives covalently bond silicon surfaces and other SEI components. AFM nano-indentation tests also suggest the alkoxy silane additives in the electrolyte function as a binder to improve silicon's ability to withstand the large reversible volume changes. The results indicate silicon surface terminations play a key role in chemical and mechanical behaviors that control reversibility.

1. Introduction

Silicon insertion anodes may be used in place of graphite for high capacity lithium-ion batteries or ultra-high capacity lithium-air batteries [1,2]. The fully lithiated $Li_{22}Si_5$ alloy has the highest theoretical capacity of any known material at 4200 mAh g^{-1} [3]; however, the large volume swelling associated with lithiation (~300%) typically causes anode pulverization and/or loss of physical contact within the anode matrix [4]. Several works have considered various types of silicon films and particles as anodes; however, these have shown limited capacities and capacity retention [1]. Recent studies demonstrate silicon nanowires are capable of withstanding the stresses of volume change with near theoretical capacities due to their unique 1D structure [5,6], and vapor–liquid–solid (VLS) grown silicon nanowires have shown capacities near 1500 mAh g^{-1} for over 80 cycles [6,7]. Likewise, Xu et al. have demonstrated the combination of silicon nanowires and conventional graphite (15% silicon nanowire by mass) allows near theoretical silicon initial capacity and maintains approximately 40% silicon capacity for at 15 cycles [8]. While the nanowire's ability to undergo reversible volume changes without pulverization is remarkable, capacity fade and particularly losses related to irreversible silicon or lithium reactions and contact losses (in composite electrodes) should be carefully considered for practical anode applications.

A key factor in maintaining reversibility is related to the solid electrolyte interphase (SEI) layer formed on the anode surface during charge/discharge cycles [9]. The SEI layer formed on graphite anodes is known to limit irreversible reactions with the electrolyte and to help maintain mechanical integrity while allowing ion transport [10–15]. The graphite SEI may be modified to improve anode performance, for example, alkoxy silane additives have been used with as surface (and the SEI) modifiers or binders to improve capacity retention [16–18]. In contrast with graphite, silicon undergoes much larger volume changes (~300%) during lithiation and delithiation steps and silicon surfaces may be relatively more reactive with the electrolyte. For example, silicon may be etched by HF (originating from $LiPF_6$ and trace water) or may react with electrolyte decomposition products to form silicon fluorides, silicon lithium alkyl carbonates and lithium silicates. In the absence of passivating SEI films (or incomplete coverage), these reactions may exacerbate capacity losses by continuously consuming active silicon through prolonged cell cycles [19–21]. In efforts to mitigate capacity losses associated with these silicon-specific reactions, several works have evaluated carbon coatings via pyrolysis, CVD, and fullerene sputtering and have shown improved initial capacities and capacity retention [22–27]. Similarly alkoxy silanes additives have been used with silicon thin film anodes and showed a two-fold increase in reversible capacity (2400 mAh g^{-1} for over 200 cycles). As with graphite, the authors attribute the improved capacity retention to the stabilization of the SEI by Si–O–Si bonding [19,28,29].

* Corresponding author at: Department of Chemical Engineering, Louisiana State University, 110 Che Bldg, South Stadium Dr, Baton Rouge, LA 70803, USA.
Tel.: +1 2255783060; fax: +1 2255781476.
E-mail address: johnflake@lsu.edu (J.C. Flake).

0378-7753/$ – see front matter © 2011 Elsevier B.V. All rights reserved.
doi:10.1016/j.jpowsour.2011.05.059

While silicon surfaces are considered more reactive, the relationships between surface chemistry and anode performance are not well established. Chan et al. describe hydride-terminated silicon surfaces as "highly reactive" and cycling nanowires with native oxides surfaces results in much lower fade and a significantly different SEI composition [7]. In addition to influencing anode stability, silicon surface chemistry also affects the transport and adsorption of lithium. Theoretical calculations based on density functional theory (DFT) show lithium transport may be hindered by a high energy barrier for insertion that may be reduced by surface modification [30–32]. In this work, we examine the role of silicon surface chemistry and consider the potential for designed or engineered solid electrolyte interfaces using silicon nanowire anodes.

2. Experimental

2.1. Sample preparation

Nanowires were prepared from single crystal (1 0 0) silicon as described in previous works [8,33,34]. Following electroless fabrication, nanowires were treated in buffered oxide etchant (BOE) and rinsed with de-ionized water to renew the hydride termination before transferring to an argon atmosphere OMNI-LAB dry box (<1 ppm water and oxygen). Anodic electrografting of methyl groups to nanowires was performed using methyl magnesium chloride as previously reported [35,36]. Siloxane functionalization of silicon nanowire was performed by immersion of silicon nanowire sample in 5% trimethoxymethylsilane in THF for 24 h in the dry box. Following functionalization, two types of silicon anodes were prepared for battery tests: nanowires attached to parent substrate (wafers) and composite silicon anodes prepared by: (1) detaching silicon nanowires from parent substrate, (2) weighing and mixing with graphite, carbon black and polyvinylidene fluoride (PVdF) in N-methylpyrrolidone (NMP) to make a paste. The paste for the composite anodes contains 15% silicon and 85% graphite by mass of the active material. The paste was applied to a copper foil via the doctor blade method and the composite anodes were dried at 120 °C for 24 h to remove excess NMP [8].

2.2. Electrochemical measurements

Silicon nanowire anodes were assembled in lithium-ion half cells with lithium foils as reference and counter electrodes. The electrolyte consisted of 1 M $LiPF_6$ (lithium hexafluorophosphate) in a 1:1 volume ratio of ethylene carbonate (EC) and dimethyl carbonate (DMC). Cyclic voltammetry was performed from 0.01 to 1.5 V versus Li/Li^+ at scan rate of 0.05 mV s^{-1} and results were normalized by geometric anode surface area. Charge/discharge measurements for composite anodes were recorded at an approximate rate of C/10 over potential range from 0.01 to 1.5 V versus Li/Li^+. Capacity data were normalized by silicon weight within composite anodes by subtracting graphite from the total anode capacity. All electrical measurements were carried out in the dry box using a Princeton PAR 2273 potentiostat.

2.3. SEI characterization

Silicon nanowire anodes were rinsed with DMC and dried in argon prior to surface characterization. The anodes were then transferred to analytical tools in sealed polyethylene containers filled with argon. SEM images were obtained using a Hitachi S-3600N variable pressure SEM system. *Ex situ* Fourier transform infra-red (FT-IR) spectroscopy in attenuated total reflectance (ATR) mode was performed using a Nicolet 6700 FT-IR system (resolution of 2 cm^{-1} for 128 scans using mercury–cadmium–telluride detector). *Ex situ* X-ray photoelectron spectroscopy (XPS) data were collected from PerkinElmer PHI 5100 system using Al Kα X-ray source with passing energy of 20 eV. Samples were sputtered with argon inside the XPS chamber to remove surface contaminants. AFM nano-indentation methods were used to determine the relative mechanical stiffness of the SEI layer on nanowire anodes. Silicon nanowire anodes were charged and discharged for 10 cycles to generate the SEI film for AFM analyses. The nanowire anodes with SEI layers were slowly contacted with a non-conductive silicon nitride tip using an Agilent 5500 AFM tool operated in contact mode. The tip approached the surface and was retracted at a constant tip-speed of 100 nm s^{-1}. Deflection was measured as a function of Z-distance from −1000 to +1000 nm using Picoscan software console. All SEM, FT-IR, XPS and AFM analyses were obtained in fully discharged condition.

3. Results and discussion

3.1. Silicon nanowire array anodes

Silicon nanowires were fabricated by electroless etching single crystal silicon wafers in aqueous hydrofluoric acid with silver nitrate solutions as described in previous studies [8,33,34]. Fig. 1 shows silicon nanowires created in this process are approximately 30 μm in length and range from 50 to 500 nm in diameter (average diameter of 253 ± 92 nm 1σ) after 30 min of electroless etching. Nitric acid was used to strip silver dendrites followed by a BOE treatment to remove oxides and provide a hydride-terminated surface (Si–H). All electrochemical measurements were carried out with nanowires attached to the bulk silicon substrate or detached from substrate and combined with graphite (in case of composite anodes). Ohmic loses across the bulk silicon substrate (500 μm thick) were negligible due to the relatively low resistivity (1–5 Ω cm) of the parent wafer.

3.2. SEI modification of silicon nanowire anodes with various surface functionalizations

Silicon nanowire arrays were prepared with three types of surface terminations: hydride-terminated (Si–H), methylated ($Si–CH_3$), and trimethoxymethylsilane treated siloxane surface (Si–O–Si–R). Another silicon anode initially hydride-terminated was cycled with 5% trimethoxymethylsilane as an additive in EC/DMC electrolyte (denoted as: "Silane Additive"), similar to

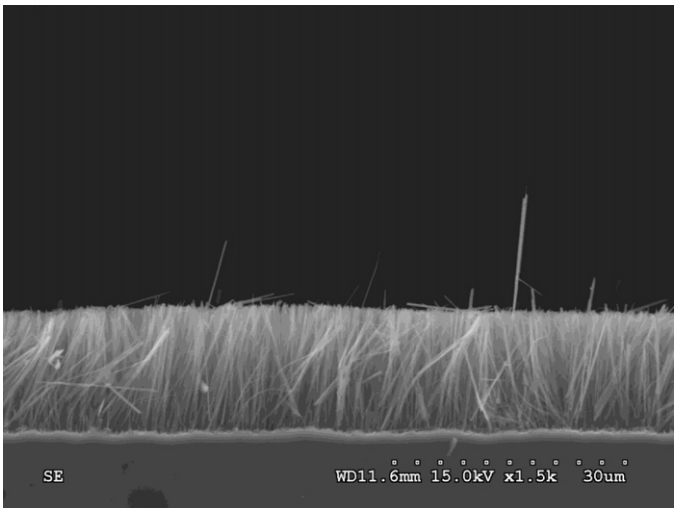

Fig. 1. SEM image of silicon nanowire arrays as fabricated.

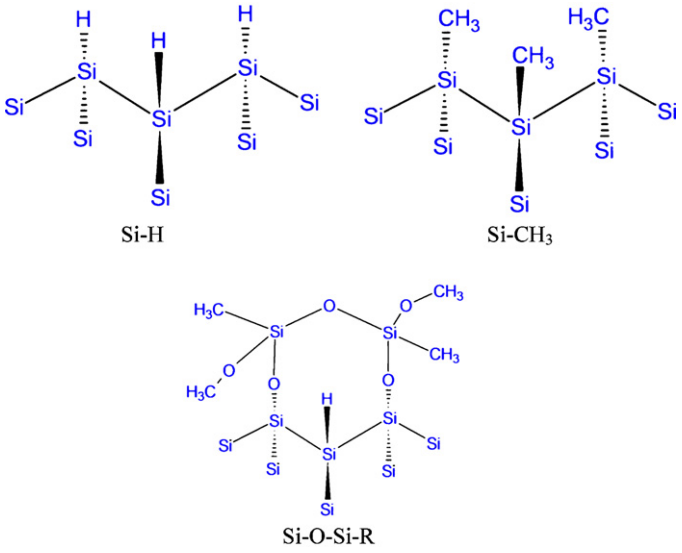

Fig. 2. Schematic representations of functionalized silicon surfaces.

previous works with thin film anodes [19]. The nanowires described here are initially crystalline and retain the (1 0 0) orientation of the parent wafer with (1 1 0) sidewalls. The three back bonds of (1 1 0) surface silicon atoms are shared with other silicon atoms and the surface bonds structures were functionalized as shown in Fig. 2.

3.3. Electrochemical measurements of silicon nanowire anodes

Cyclic voltammograms for the first cycle (from 1.5 to 0.01 V versus Li/Li^+) are shown in Fig. 3. The nanowire anode which was initially hydride-terminated (Si–H) shows charge peaks at approximately 0.4–0.6 V versus Li/Li^+, corresponding to electrolyte reduction. The charging current increases sharply at potentials more cathodic than 0.2 V which corresponds with lithium insertion. When trimethoxymethylsilane is added to the electrolyte with the hydride-terminated nanowire anodes, current densities increase significantly and reach a maximum of approximately 0.17 mA cm^{-2} near 0.1 V versus Li/Li^+ consistent with lithiation. Both the methyl-terminated ($Si–CH_3$) and siloxane-terminated (Si–O–Si–R) anodes show low current densities (less than 0.04 mA cm^{-2}) at all potentials without significant lithiation currents. All four anodes show relatively low discharge currents, which may be due to nanowire

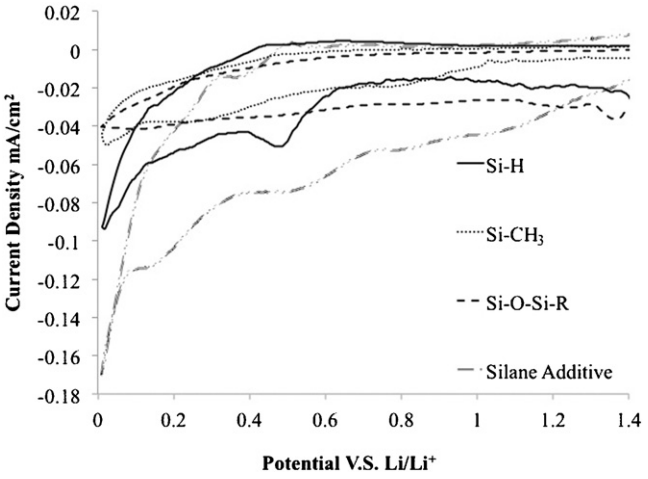

Fig. 3. Cyclic-voltammograms of various silicon nanowire anodes.

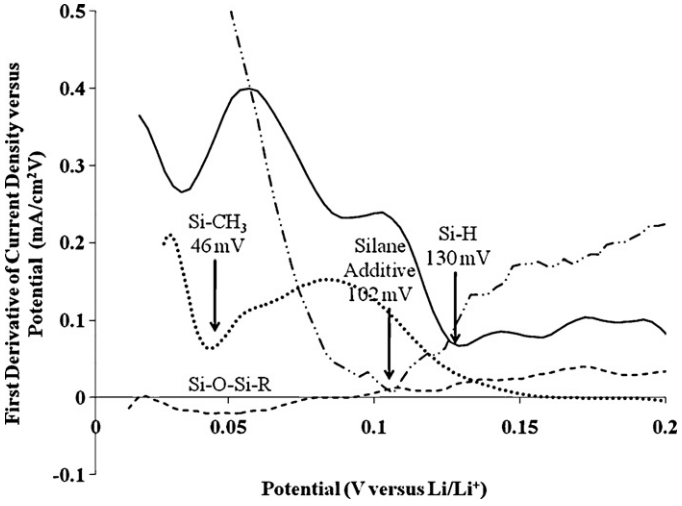

Fig. 4. Onset potentials for silicon nanowire anodes derived from voltammograms.

agglomeration (observed after the reactions) and possible mechanical failures between nanowires and substrates.

Lithiation onset potentials may be estimated from the derivative of current versus potential curves (based on the voltammograms shown in Fig. 3). As shown in Fig. 4, more cathodic onset potentials for lithium insertion are associated with higher energy barriers for lithium adsorption and transport [30–32]. Lithiation potentials for silicon nanowires with surface oxides appears near 200 mV versus Li/Li^+, which can be explained by favorable silicon oxide surface intercalation with lithium [7]. The lithiation potential for the hydride-terminated silicon anode occurs at potentials near 130 mV versus Li/Li^+ mV which is the most anodic among all four anodes considered here. When 5% trimethoxymethylsilane additives were added, Si–O–Si crosslinking occurs and the lithiation onset potential shifts cathodically to approximately 102 mV, suggesting a higher barrier for adsorption. The onset potential for the directly methylated silicon anode occurs near 46 mV, suggesting lithium insertion into silicon may be hindered due to the passivating nature of the methyl group [36]. The siloxane-terminated silicon anode shows no obvious onset potential for lithiation similar to methylated surface.

3.4. SEI characterization

3.4.1. FT-IR analyses

As reported in anode studies with graphite [14] and silicon [19], FT-IR analyses can provide useful information regarding the composition of SEI. *Ex situ* FT-IR analyses (ATR mode) of silicon nanowire anode surfaces after the first charge/discharge cycle are presented in Fig. 5. Peak assignments were made using standards created in the lab or using published FT-IR spectra [14,19,37].

Hydride-terminated (Si–H) nanowire anodes show several new absorption peaks after the first charge/discharge cycles which are associated with the SEI (Fig. 5, top). The doublet near 854–841 cm^{-1} may be assigned as Li–F (850 cm^{-1}) from the decomposition of $LiPF_6$. Likewise, P–F stretching (850–800 cm^{-1}) is also observed and is associated with inorganic $LiPF_x$ and $LiPF_xO$ compounds. The peak centered near 1635 cm^{-1} suggests the presence of lithium or silicon alkyl carbonates ($R–OCO_2^-M^{n+}$, where M represents Li–Si alloy and R is an alkyl group). Similarly, the doublet at 1482, 1418 cm^{-1} and the peak near 1071 cm^{-1} are attributed to $CH_3CH_2–$, C=O and C–O moieties (respectively) from these carbonates. The C–H bending seen at 1304 and 1211 cm^{-1} is also associated with alkyl carbonates within the SEI.

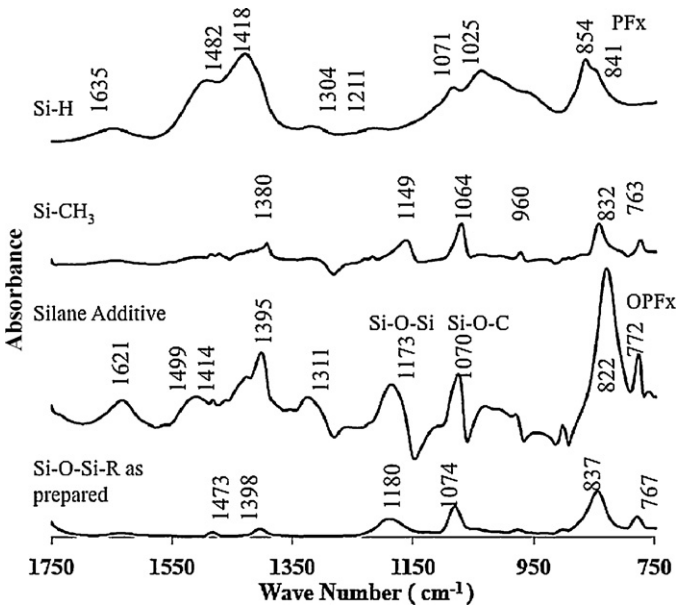

Fig. 5. FT-IR spectra of SEI on silicon nanowire anodes.

Relative to the hydride-terminated nanowires (including those cycled with the alkoxy silane additives) spectra from the methylated nanowires (Si–CH_3) show fewer new peaks arising from the first charge/discharge cycle (Fig. 5 second spectra from top). A diminished characteristic peak at 832 cm^{-1} is attributed to residual $LiPF_6$. In contrast with hydride-terminated surfaces show that carbonate decomposition, the peaks at 1380, 1149, 1064, 960 and 760 cm^{-1} can be assigned to the EC/DMC electrolyte itself. There are no measurable peaks near 1633 cm^{-1} for R–$OCO_2{}^-M^{n+}$ groups. These results suggest the methyl monolayer on silicon surface is relatively un-reactive with the electrolyte at potentials up to 0.01 V versus Li/Li^+.

As seen in the hydride-terminated nanowire cycled with silane additive spectra (Fig. 5 third spectra from top) there are a number of new peaks particularly those associated with Si–O–Si species and OPFx compounds. The strong peaks at approximately 822 and 772 cm^{-1} are associated with P–F stretching (850–800 cm^{-1}) and P–O–C (830–740 cm^{-1}) stretching from O=PF–OR compounds, as well as C–O bending (846–740 cm^{-1}) for Li_2CO_3 formed in SEI. The absorption peak at 1621 cm^{-1} arises from carbonyl groups, R–$OCO_2{}^-M^n$; and peaks at 1499, 1414, 1311 and 1173 cm^{-1} are attributed to $CH_3CH_2{}^-$, C=O, C–H and C–O from carbonates, respectively. Si–O–Si stretching and Si–O–C stretching peaks are also seen at 1173 cm^{-1} and at 1070 cm^{-1}, respectively.

While the methylated surface appears unreactive, the Si–H anode shows active SEI formation including lithium or silicon alkyl carbonates, lithium salts and P-F containing species. The formation of PF containing products may originate from $LiPF_6$ decomposition to LiF and PF_5. PF_5 is strong Lewis acid and reacts with trace water to form O=PF_3 and HF.

$$PF_5 + H_2O \Rightarrow O{=}PF_3 + HF$$

The HF and O=PF_3 may then react with lithium to from LiF and P–F species. When hydride-terminated silicon anodes are cycled with trimethoxymethylsilane additives, the only significant differences between the hydride-terminated spectra and the same anodes with trimethoxymethylsilane additives are the generation of Si–O–Si bonds and new organic phosphorous fluorine compounds. This Si–O–Si bond is likely formed through hydrolysis and condensation with the presence of water and Li^+, and the overall reaction can be expressed as [16]:

$$RSiOCH_3 + R'SiOCH_3 \overset{H_2O,Li^+}{\Rightarrow} RSiOSiR' + CH_3OH$$

$$O{=}PF_3 + {\bullet}OCH_3 \overset{Li^+}{\Rightarrow} O{=}PF_2OCH_3 + LiF$$

When trimethoxymethylsilane additives are used, more methoxy groups are introduced and reactions with OPF_3 may lead to organic phosphorous fluorine compound as observed by FT-IR analyses.

FT-IR spectra of siloxane-terminated anodes (Si–O–Si–R) as prepared shows absorption peaks arising from alkyl and Si–O species (Fig. 5, bottom). Peaks at 1473 and 1398 cm^{-1} may be attributed C–H bending from methyl groups. Peaks at 1180 and 1174 cm^{-1} can be assigned as Si–O–Si and Si–O–C stretches, respectively. The strong peak at 837 cm^{-1} is from Si–C stretching, and the peak at 767 cm^{-1} is Si–O–Si symmetric stretch. FT-IR spectra of siloxane-terminated silicon anodes after cycling is similar to the silicon anode cycled with 5% trimethoxymethylsilane additives in EC/DMC electrolyte.

3.4.2. XPS analyses

Carbon, oxygen, fluorine, and silicon XPS spectra of silicon nanowire anodes after the first cell cycle are shown in Fig. 6. Peaks are assigned using standards or previous silicon and graphite anode XPS studies [7,13,20].

The C (1s) spectra of silicon anodes with methylated-termination in Fig. 6 shows a broad peak from 286.2 indicating the presence of C–O, C=O in carbonate and/or Si–C of Si–CH_3 surface. The O (1s) peak at 534.2 eV can be attributed to hydrocarbons. The strong peak at approximately 688.2 eV for F (1s) suggests $LiPF_6$ residues. As with the FT-IR analysis, the XPS data indicate the surface of methylated silicon anodes is relatively unreactive and primarily includes electrolyte residuals in addition to the grafted layer.

The C (1s) spectra of hydride-terminated silicon anodes (Fig. 6 bottom spectra) shows a shoulder from 286 to 288 eV suggesting the presence of C–O, C=O in carbonates, while a peak at 291 eV corresponds to organoflourine compounds. The O (1s) peak at 532.8 eV can be attributed to O in carbonates. A strong peak at 686.4 eV for F (1s) suggests C–F bonds from fluorocarbons and LiF, which are consistent with C (1s) spectrum.

When 5% trimethoxymethylsilane is added to electrolyte with hydride-terminated nanowires, the C (1s), O (1s) and F (1s) spectra of the SEI (Fig. 6 middle spectra) were similar to the hydride-terminated silicon anodes without any additives suggesting similar composition for C, O and F species. As shown in Fig. 7, the SEI is enriched with Si species. Bare (uncycled) silicon nanowire Si (2p) spectra typically show two peaks at 99.2 and 103.6 eV corresponding to silicon and native oxides; while that of silicon anodes cycled with trimethoxymethylsilane additives show these peaks are shifted to 99.3 and 104.3 eV indicating Si–O–Si and Si–O–C bonds are formed when silanes are added to the electrolyte.

Significant quantities of fluorocarbons are observed in the SEI on silicon anodes both with and without trimethoxymethylsilane additives in this work as well as reported in previous studies [7,20]. Fluorocarbons are associated with silicon anodes (not typically observed at graphite anodes) and indicate reactions associated with both silicon and electrolyte. Yen et al. have proposed that fluorocarbon compounds are generated from the reactions between the $SiF_6{}^{-2}$ and hydrocarbons [20]; however, it seems unlikely that $SiF_6{}^{-2}$ species are capable of transferring fluorine to hydrocarbons (ΔG_f = −525.7 kcal mol^{-1} [38]). A more likely scenario would indicate that silicon participates in fluorocarbon formation. It is

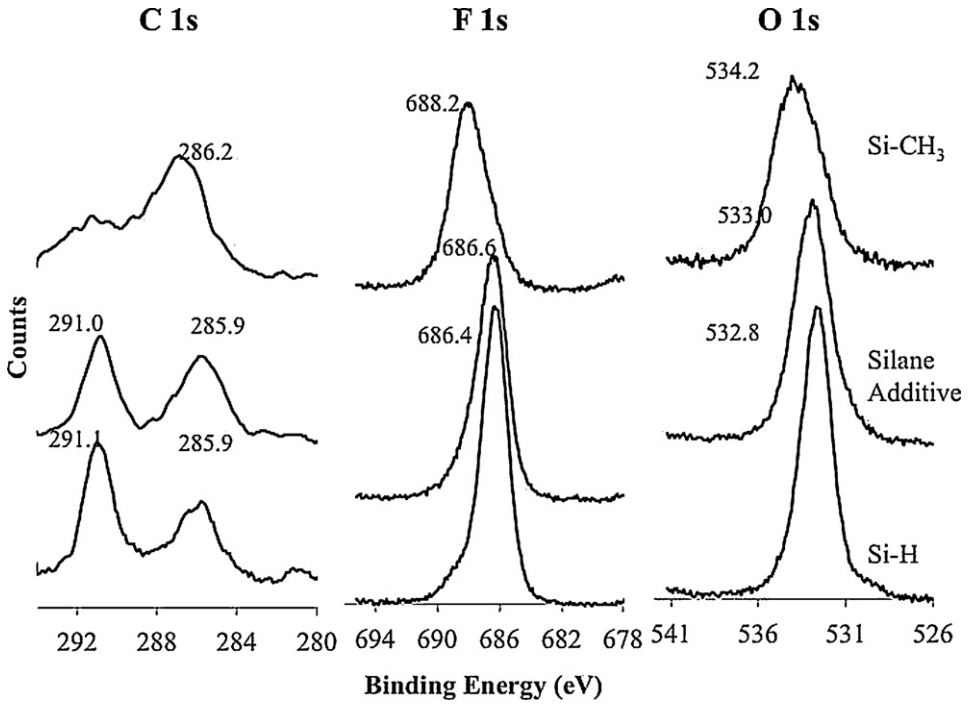

Fig. 6. XPS spectra of SEI on silicon nanowire anodes.

possible alkyl carbonate radicals may react with fluorophosphates to generate fluorocarbon compounds rather than bonding with silicon surfaces as is possible with graphite.

Although the anode performance may be strongly affected with trimethoxymethylsilane additives (as described in the next section), FT-IR spectra and XPS spectra from pretreated siloxane-terminated anodes (rather than adding silanes to the electrolyte) is similar to the silicon anode cycled with the additives. This suggests excess trimethoxymethylsilane additives in the electrolyte do not alter the surface chemistry of the SEI.

3.5. Charge/discharge test for silicon nanowire composite anodes

While silicon nanowires attached to their parent wafer offer homogeneous substrates for analytical purposes, their use as reversible anodes is severely limited due to agglomeration and contact loss upon cycling. For this reason, the capacity and cycle performance of functionalized silicon anodes using composite anodes have been evaluated. Silicon nanowire composite anodes (15% silicon nanowires and 85% graphite [8]) including Si–H, Si–CH_3, and Si–O–Si–R functionalized nanowire anodes were prepared and cycled in lithium-ion half cells. Another hydride-terminated silicon nanowire composite anode was also cycled in with 5% trimethoxymethylsilane additive under the same conditions.

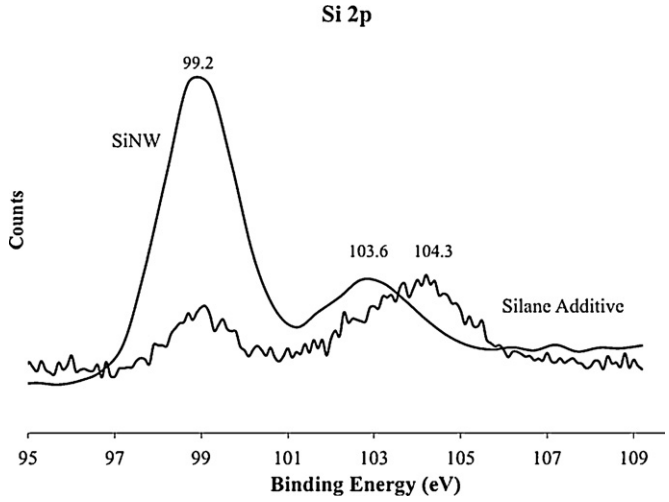

Fig. 7. XPS Si (2p) spectra of SEI on silicon nanowire anodes cycled with silane additive and bare silicon nanowire.

As seen in the SEM images, silicon nanowires are randomly distributed among graphite flakes in the composite anode as prepared (Fig. 8A). The anode surface is covered with an observable organic layer after 15 charge/discharge cycles as shown in Fig. 8B.

The discharge specific capacities versus cycle number for composite anodes are shown in Fig. 9. In this case discharge capacities are normalized to silicon specific capacities by subtracting graphite capacities within anodes. The initial discharge capacity for hydride-terminated silicon composite anode is 2433 mAh g^{-1}. The same anode shows a reversible capacity of approximately 1364 mAh g^{-1} after 15 cycles with a capacity fade of 5.7% per cycle. The methylated composite anode shows a significantly lower initial specific discharge capacity of 538 mAh g^{-1} and a reversible capacity of 383 mAh g^{-1} after 15 cell cycles. The Si–O–Si–R composite anode shows slightly higher initial discharge capacity at 1087 mAh g^{-1}, and reversible capacity at 368 mAh g^{-1}. The reversible capacities for Si–CH_3 and Si–O–Si–R composite anodes are significantly lower than that of Si–H, suggesting silicon capacities are compromised by these functionalizations. Hydride-terminated silicon nanowire composite anodes cycled with trimethoxymethylsilane additives shows the greatest initial discharge capacity at 3287 mAh g^{-1} and the great reversible capacity of 2348 mAh g^{-1} after 15 cell cycles. While the performance of the hydride-terminated nanowire anodes with the additives is significantly better than other functionalized electrodes, the FT-IR or XPS showed minor changes in the SEI composition besides increases in Si–O–Si bonds and organic phosphorous fluorine compounds. Moreover, a cathodic shift in onset potential was observed when silanes were added to electrolyte with Si–H anodes indicating higher energy barrier for

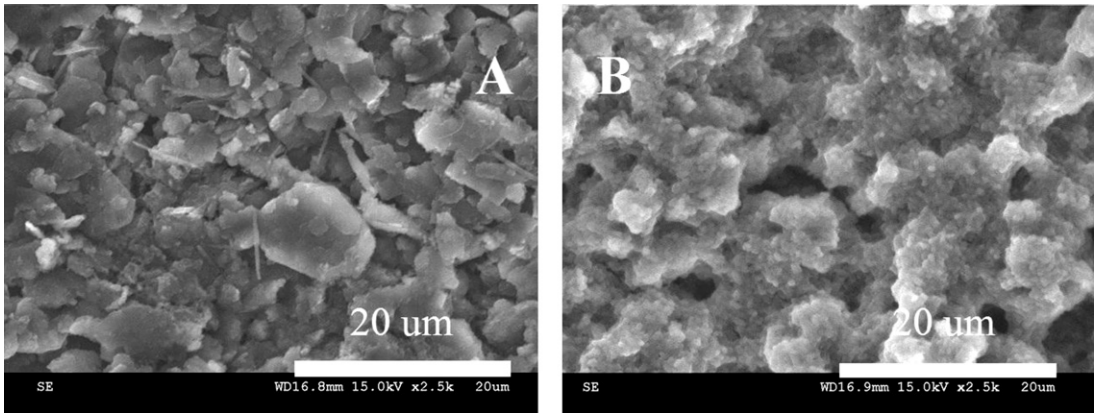

Fig. 8. SEM images of silicon nanowire composite anodes (A) before and (B) after cycling.

lithium insertion. While the initial capacities are somewhat similar, the 75% increase in reversible capacity associated to hydride-terminated nanowire cycled is remarkable and suggest the alkoxy silane additives improve capacity retention via a mechanical mechanism.

3.6. AFM nano-indentation on SEI

An AFM nano-indentation was used to evaluate mechanical properties of the SEI film on silicon nanowires based on the notion that the chemical nature of the silane-derived SEI layer is not the primary factor attributing to improved anode capacity and capacity, In fact, several reports suggest the improvement in capacity retention is associated with mechanical improvements; however, there are no quantitative data to support the conclusion [39,40]. SPM (scanning probe microscopy) and AFM analyses have been used to study the morphology of SEI layers on graphite, tin and silicon anodes for lithium-ion batteries [41–44]; however the mechanical properties of SEI are not studied extensively. AFM has also been used to determine mechanical properties of polymeric materials and thin organic films such as elastic modulus and contact stiffness via nano-scale indentation [45–47]. Fig. 10 shows external load versus depth profiles of SEI layers on Si–H anode and hydride-terminated silicon anode cycled with 5% trimethoxymethylsilane additives using nano-indentation analyses. The slope of external load versus depth profile can be related to the surface contact stiffness of the SEI layer. The contact stiffness of SEI on hydride-terminated silicon anode cycled with trimethoxymethylsilane additives (0.9568 N m^{-1}) is approximately 125% greater than that of SEI without silane additive (0.429 N m^{-1}). The higher contact stiffness suggests silicon crosslinking within the SEI which may be associated with improved adhesion within the anode matrix as binders.

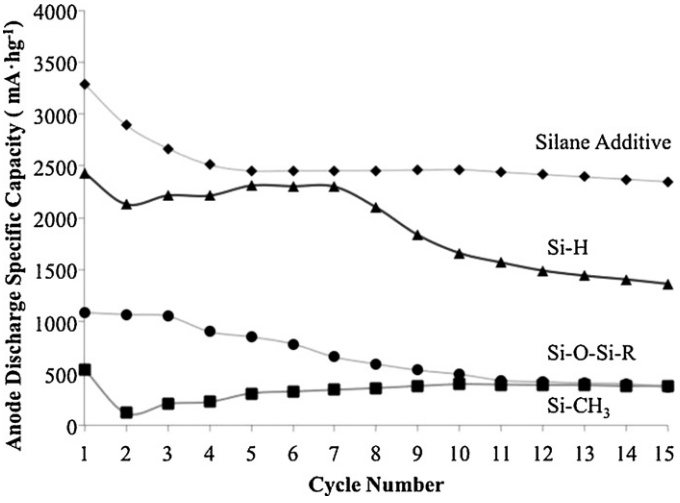

Fig. 9. Discharge capacities versus cycle number of various silicon nanowire composite anodes.

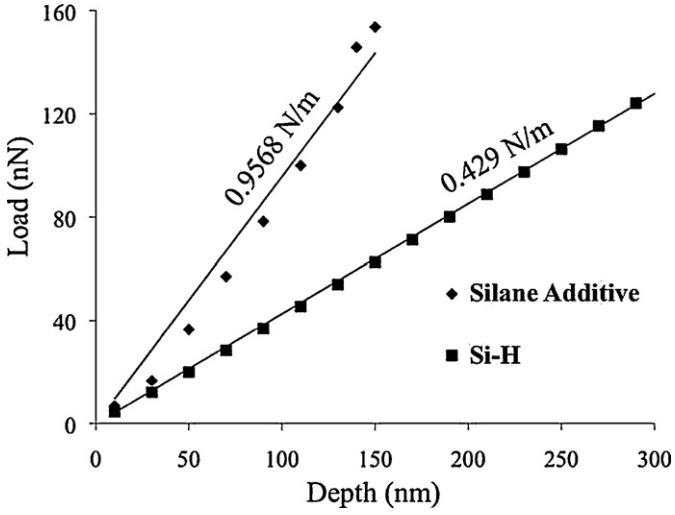

Fig. 10. External loads versus Z-depth profiles for SEI layers on hydride-terminated silicon anodes and silicon anodes cycled with silane additive obtained via AFM nano-indentation analysis.

4. Conclusions

Silicon nanowire anodes with hydride, methylated, siloxane terminated surfaces were prepared and their SEI layers were characterized by cyclic voltammetry, FT-IR, XPS and AFM analyses. Vibrational and binding energies show methylated silicon nanowires are relatively unreactive while hydride-terminated silicon nanowire show SEI layers include carbonates, lithium salts, P–F species and fluorocarbon compounds. Lithiation potentials appear to be a strong function of surface chemistry, for example the hydride-terminated silicon anode on-set potential is 104 mV, while that of methylated anode is 46 mV versus Li/Li$^+$. Pre-treating nanowires with trimethoxymethylsilane and adding trimethoxymethylsilane to the electrolyte show similar SEI compositions, including Si–O–Si groups and OPFx species, however, capacity retention with trimethoxymethylsilanes added to the electrolyte are remarkably higher. Charge/discharge capacities

of composite anodes show reversible silicon specific capacity is increased by approximately 75% (2348 mAh g^{-1}) when 5% trimethoxymethylsilane is used as an additive compared to hydride terminated anodes after 15 cycles. While the FT-IR and XPS analyses show no significant difference in chemical composition in the SEI between anodes pretreated with versus alkoxy silanes added to the electrolyte; AFM nano-indentation analyses show contact stiffness is 125% greater with the additive in the electrolyte. The results suggest the primary benefit of the trimethoxymethylsilane additives is associated with mechanical (adhesion) improvements as a binder within the SEI that increases silicon's ability to undergo the large volume change associated with lithiation/delithiation cycling. These results suggest surface terminations or additives that improve the adhesion or binding properties allowing reversible cycling while passivating surfaces hinder lithiation as well as side reactions. The work shows the potential for engineering silicon-SEI interfaces to tune or optimize chemical and mechanical properties for improved reversibility.

References

[1] U. Kasavajjula, C. Wang, A.J. Appleby, Journal of Power Sources 163 (2007) 1003–1039.
[2] G. Cohn, D. Starosvetsky, R. Hagiwara, D.D. Macdonald, Y. Ein-Eli, Electrochemistry Communications 11 (2009) 1916–1918.
[3] H. Okamoto, Journal of Phase Equilibria 11 (1990) 306–312.
[4] A. Anani, S. Crouch-Baker, R.A. Huggins, Journal of the Electrochemical Society 134 (1987) 3098–3102.
[5] U. Kasavajjula, C.S. Wang, A.J. Appleby, Journal of Power Sources 163 (2007) 1003–1039.
[6] C.K. Chan, H.L. Peng, G. Liu, K. McIlwrath, X.F. Zhang, R.A. Huggins, Y. Cui, Nature Nanotechnology 3 (2008) 31–35.
[7] C.K. Chan, R. Ruffo, S.S. Hong, Y. Cui, Journal of Power Sources 189 (2009) 1132–1140.
[8] W.L. Xu, J.C. Flake, Journal of the Electrochemical Society 157 (2010) A41–A45.
[9] E. Peled, D. Goloditsky, D.J. Penciner, J.O. Besenhard, Handbook of Battery Materials, 1999.
[10] E. Peled, H. Yamin, Israel Journal of Chemistry 18 (1979) 131–135.
[11] F. Kong, R. Kostecki, G. Nadeau, X. Song, K. Zaghib, K. Kinoshita, F. McLarnon, Journal of Power Sources 97-8 (2001) 58–66.
[12] A.V. Churikov, Electrochimica Acta 46 (2001) 2415–2426.
[13] H. Bryngelsson, M. Stjerndahl, T. Gustafsson, K. Edstr, Journal of Power Sources 174 (2007) 970–975.
[14] a.Y.W. Perla, B. Balbuena, Lithium-Ion Batteries: Solid-Electrolyte Interphase, Imprerial College Press, London, 2004.
[15] J.M. Tarascon, M. Armand, Nature 414 (2001) 359–367.
[16] G. Schroeder, B. Gierczyk, D. Waszak, M. Walkowiak, Electrochemistry Communications 8 (2006) 1583–1587.
[17] K. Amine, Q. Wang, D.R. Vissers, Z. Zhang, N.A.A. Rossi, R. West, Electrochemistry Communications 8 (2006) 429–433.
[18] S.B. Ng, J.Y. Lee, Z.L. Liu, Journal of Power Sources 94 (2001) 63–67.
[19] S.W. Song, S.W. Baek, Electrochemical and Solid State Letters 12 (2009) A23–A27.
[20] Y.C. Yen, S.C. Chao, H.C. Wu, N.L. Wu, Journal of the Electrochemical Society 156 (2009) A95–A102.
[21] N.S. Choi, K.H. Yew, H. Kim, S.S. Kim, W.U. Choi, Journal of Power Sources 172 (2007) 404–409.
[22] H.S. Kim, K.Y. Chung, L.W. Cho, Bulletin of the Korean Chemical Society 29 (2008) 1965–1968.
[23] R. Huang, X. Fan, W.C. Shen, J. Zhu, Applied Physics Letters 95 (2009).
[24] J. Xiao, W. Xu, D.Y. Wang, D.W. Choi, W. Wang, X.L. Li, G.L. Graff, J. Liu, J.G. Zhang, Journal of the Electrochemical Society 157 (2010) A1047–A1051.
[25] Y. Yu, L. Gu, C.B. Zhu, S. Tsukimoto, P.A. van Aken, J. Maier, Advanced Materials 22 (2010) 2247.
[26] L.F. Cui, Y. Yang, C.M. Hsu, Y. Cui, Nano Letters 9 (2009) 3370–3374.
[27] A.A. Arie, O.M. Vovk, J.K. Lee, Journal of the Electrochemical Society 157 (2010) A660–A665.
[28] C.C. Nguyen, S.W. Song, Electrochimica Acta 55 (2010) 3026–3033.
[29] Y.G. Ryu, S. Lee, S. Mah, D.J. Lee, K. Kwon, S. Hwang, S. Doo, Journal of the Electrochemical Society 155 (2008) A583–A589.
[30] B. Peng, F.Y. Cheng, Z.L. Tao, J. Chen, Journal of Chemical Physics 133 (2010).
[31] Q.F. Zhang, W.X. Zhang, W.H. Wan, Y. Cui, E.G. Wang, Nano Letters 10 (2010) 3243–3249.
[32] K.C. Maria, G. Jeffrey, ECS Meeting Abstracts 1003 (2010) 58.
[33] K.Q. Peng, Y.J. Yan, S.P. Gao, J. Zhu, Advanced Materials 14 (2002) 1164–1167.
[34] K.Q. Peng, Y.J. Yan, S.P. Gao, J. Zhu, Advanced Functional Materials 13 (2003) 127–132.
[35] J.N. Ngunjiri, S.S.S. Vegunta, J.C. Flake, Journal of the Electrochemical Society 156 (2009) H516–H521.
[36] S.S.S. Vegunta, J.N. Ngunjiri, J.C. Flake, Langmuir 25 (2009) 12750–12756.
[37] W.A.v.S.a.B. Scrosati, Advances in Lithium-ion Batteries, Kluwer Academic/Plenum Publisher, New York, 2002.
[38] J.C.A.S.C.D. Schaeffer, M.W. Thomsen, C.H. Yoder, Data for General, Inorganic, Organic, and Physical Chemistry, 1989.
[39] D. Aurbach, B. Markovsky, I. Weissman, E. Levi, Y. Ein-Eli, Electrochimica Acta 45 (1999) 67–86.
[40] S. Menkin, D. Golodnitsky, E. Peled, Electrochemistry Communications 11 (2009) 1789–1791.
[41] D. Alliata, R. Kotz, P. Novak, H. Siegenthaler, Electrochemistry Communications 2 (2000) 436–440.
[42] M. Inaba, H. Tomiyasu, A. Tasaka, S.K. Jeong, Z. Ogumi, Langmuir 20 (2004) 1348–1355.
[43] S. Leroy, F. Blanchard, R. Dedryvere, H. Martinez, B. Carre, D. Lemordant, D. Gonbeau, Surface and Interface Analysis 37 (2005) 773–781.
[44] I.T. Lucas, E. Pollak, R. Kostecki, Electrochemistry Communications 11 (2009) 2157–2160.
[45] M.R. Vanlandingham, S.H. McKnight, G.R. Palmese, J.R. Elings, X. Huang, T.A. Bogetti, R.F. Eduljee, J.W. Gillespie, The Journal of Adhesion 64 (1997) 31–59.
[46] M.R. VanLandingham, J.S. Villarrubia, W.F. Guthrie, G.F. Meyers, Macromolecular Symposia 167 (2001) 15–43.
[47] M. Wyart, H. Liang, A. Kabla, L. Mahadevan, Physical Review Letters 101 (2008) 215501.